JCTC Journal of Chemical Theory and Computation

Article

pubs.acs.org/JCTC

A Multidimensional B-Spline Correction for Accurate Modeling Sugar Puckering in QM/MM Simulations

Ming Huang, Thakshila Dissanayake, Erich Kuechler, Brian K. Radak, Tai-Sung Lee, Timothy J. Giese, and Darrin M. York*

Center for Integrative Proteomics Research, Laboratory for Biomolecular Simulation Research and Department of Chemistry and Chemical Biology, Rutgers University, 174 Frelinghuysen Road, Piscataway, New Jersey 08854, United States

Supporting Information

ABSTRACT: The computational efficiency of approximate quantum mechanical methods allows their use for the construction of multidimensional reaction free energy profiles. It has recently been demonstrated that quantum models based on the neglect of diatomic differential overlap (NNDO) approximation have difficulty modeling deoxyribose and ribose sugar ring puckers and thus limit their predictive value in the study of RNA and DNA systems. A method has been introduced in our previous work to improve the description of the sugar puckering conformational landscape that uses a multidimensional B-spline correction map (BMAP correction) for systems involving intrinsically coupled torsion angles. This method greatly improved the adiabatic potential energy surface profiles of DNA and RNA sugar rings relative to high-level *ab initio* methods even for highly problematic NDDO-based models. In the present work, a BMAP correction is developed, implemented, and tested in molecular dynamics simulations using the AM1/d-PhoT semiempirical Hamiltonian for biological phosphoryl transfer reactions. Results are presented for gas-phase adiabatic potential energy surfaces of RNA transesterification model reactions and condensed-phase QM/MM free energy surfaces for nonenzymatic and RNase A-catalyzed transesterification reactions. The results show that the BMAP correction is stable, efficient, and leads to improvement in both the potential energy and free energy profiles for the reactions studied, as compared with *ab initio* and experimental reference data. Exploration of the effect of the size of the quantum mechanical region indicates the best agreement with experimental reaction barriers occurs when the full CpA dinucleotide substrate is treated quantum mechanically with the sugar pucker correction.

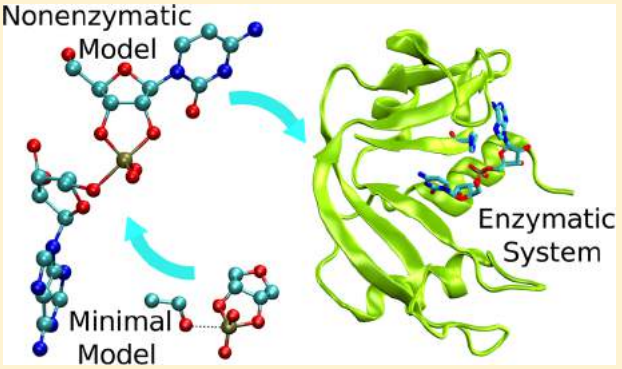

INTRODUCTION

Sugar rings are important components of carbohydrates and nucleic acids.[1,2] The ribose five-membered ring in RNA forms a key structural link between the phosphate backbone and nucleobase,[3] and it can adopt several characteristic conformational states (sugar puckering modes) that can influence the structure and function of nucleic acids.[4−8] Considerable effort has been devoted to the study of sugar ring conformation energy profiles with molecular simulations and quantum mechanical methods, including approximate density-functional and semiempirical models.[9−14] Torsion angle rotational barriers are particularly problematic for semiempirical methods based on the neglect of diatomic differential overlap (NDDO) approximation.[14−17] Very recently, we performed a computational study of sugar pucker potential energy surfaces, and we introduced a nonelectronic correction to semiempirical models to improve their quality with respect to MP2 results.[16] Sugar pucker corrections were implemented using a multidimensional B-spline correction method[16] (BMAP correction) for coupling the torsion angle energy terms. The BMAP correction has the advantage of being robust with respect to data noise. It has simple and efficient analytic derivatives, and it can be more easily extended to higher dimensions than methods based on cubic spline interpolation.[18−22] The BMAP correction strategy has been adopted by others, who have successfully extended it to improve sugar pucker profiles in the nicotinamide ribonucleoside.[14] Recent orthogonalization-corrected semiempirical methods also have the potential to provide good treatment to sugar ring conformations.[23]

In the present work, BMAP-corrected semiempirical methods, particularly AM1/d-PhoT,[24] are applied to the cytidilyl-3′,5′-adenosine (CpA) RNA transesterification reaction in solution[17,25−28] and in the presence of the RNase A protein enzyme.[29−32] First, we compare *ab initio* and semiempirical quantum mechanical (QM) Hamiltonians by examining two-dimensional (2D) gas-phase potential energy surfaces (PESs) of a minimal model reaction of CpA. These comparisons are made with and without the inclusion of the BMAP correction to the AM1/d-PhoT[24] and DFTB3−3ob/

Received: February 14, 2017
Published: August 2, 2017

DOI: 10.1021/acs.jctc.7b00161
J. Chem. Theory Comput. XXXX, XXX, XXX−XXX

OPhyd semiempirical models.[16,24,33] Second, one-dimensional (1D) potential of mean force (PMF) profiles of the CpA RNA transesterification reaction are computed in solution using hybrid quantum mechanical/molecular mechanical (QM/MM) AM1/d-PhoT simulations, both with and without the BMAP-correction. Third, 2D PMF QM/MM profiles of the CpA RNA transphosphorylation reaction is computed in the presence of the RNase A protein enzyme. We perform the 1D and 2D PMFs multiple times using different definitions of the QM region to explore the sensitivity of the reaction profiles to this choice. Furthermore, we monitor the distribution of CpA sugar puckers with the AMBER FF10 force field and compare those distributions to QM/MM simulations performed with and without the BMAP correction.

The AM1/d-PhoT QM/MM simulations with the BMAP correction are found to more closely resemble the sugar pucker distributions observed in MM simulations, and the BMAP correction improves the reaction barriers in comparison to *ab initio* QM results. These results demonstrate that the BMAP sugar pucker correction will be useful in the study of RNA systems in condensed phase using QM/MM simulations with semiempirical QM methods.

COMPUTATIONAL METHODS

Figure 1 displays the three systems examined in the present work, and Figure 2 illustrates the QM regions used in the QM/MM simulations. Figure 1a is the minimal model reaction used to construct 2D gas-phase adiabatic potential energy surfaces. Specifically, this reaction involves the departure of ethoxide (EthO) leaving group from a 2′,3′-cyclic sugar phosphate (SP), and we refer to this reaction by "EthO···SP". Figure 1b is the CpA RNA used to produce QM/MM 1D PMFs of the transesterification reaction in solution. The 1D PMFs are recomputed using the CpA_TQM (truncated QM) and CpA_FQM (full QM) QM regions shown in Figure 2. Figure 1c is the CpA in the presence of the RNase A protein enzyme used when generating 2D PMFs. The 2D PMFs are recomputed using the RNaseA_TQM and RNaseA_FQM QM regions shown in Figure 2.

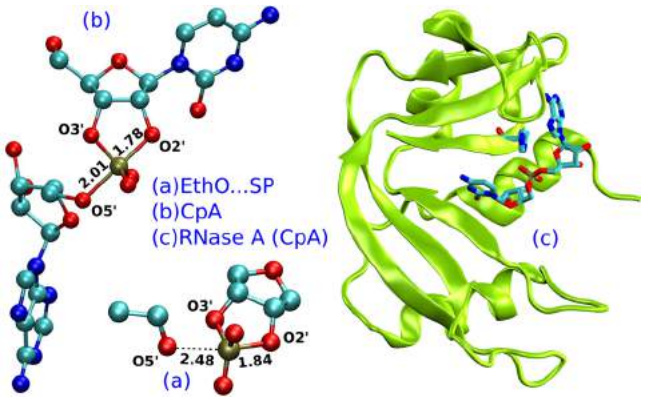

Figure 1. Transition states of the RNA transesterification reaction models and RNase A system. (Only nonhydrogen "heavy" atoms are shown). (a) Minimal EthO···SP model used to construct 2D adiabatic PESs in the gas-phase; optimized MP2 transition state shown. (b) Full dinucleotide (CpA) nonenzymatic model. (c) RNase A enzyme complexed with CpA. Labeling of the O2′, O3′, and O5′ positions follows the conventions used in RNA, and lengths are given for the nucleophile (P−O2′) and leaving group (P−O5′) bonds.

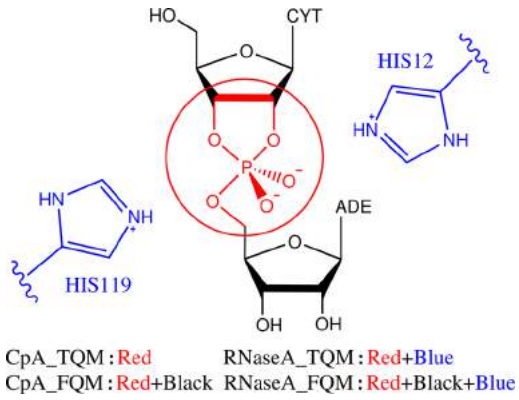

Figure 2. QM regions used in the QM/MM simulations. TQM and FQM denote truncated and full QM regions, respectively. The histidines are RNase A residues and they are, therefore, not present in the nonenzymatic simulations of CpA.

All simulations and semiempirical calculations were performed with a development version of the AMBER14 software package,[34] and all *ab initio* QM calculations were performed with the Gaussian 09 program.[35] The PMF surfaces were computed from the umbrella window simulations using the variational free energy perturbation (vFEP) method.[36,37] Unlike the weighted histogram analysis method, vFEP does not require significant overlap of the probability density between adjacent umbrella window simulations to achieve smooth and robust PMFs. We have, nevertheless, included demonstrations in the Supporting Information emphasizing that we do, in fact, achieve significant overlap between our simulations.

2D Potential Energy Surfaces of the Minimal Model Reaction. Figure 3 compares the 2D gas-phase adiabatic PESs of the EthO···SP minimal model reaction between various *ab initio* and semiempirical QM models. The coordinates are the forming (P−O2′) and breaking (P−O5′) bond lengths, and the isocontour values are kcal/mol. The black dots are stationary points. The MP2, M062X, and B3LYP *ab initio* results were geometry optimized with the 6-31++G(d,p) basis, and the energy was refined using the 6-311++G(3df,2p) basis. AM1/d and DFTB3-OP refer to the AM1/d-PhoT[24] and DFTB3-3ob/OPhyd[33] semiempirical Hamiltonians, respectively. AM1/d +E_{corr} and DFTB3-OP+E_{corr} denote the use of the BMAP sugar pucker correction. The white lines appearing in Figure 3 are nudged elastic band[38] (NEB) minimum energy pathways optimized on the 2D surface. The structure of each transition state (TS) is shown above each PES, and the sugar's pseudorotation phase angle P_θ and amplitude A_r are shown in parentheses.

The nomenclature for describing pseudorotation is illustrated in Figure 4. In brief, the pseudorotation phase angle P_θ and amplitude A_r are related to the proper torsions of the sugar ν. These two values can be interpreted as a pair of polar coordinates (A_r,P_θ) defining the precise location of the sugar pucker within the pseudorotation wheel. Alternatively, the location can be equivalently described using a set of Cartesian coordinates (Z_x,Z_y).[16]

To generate the BMAP corrections used in the AM1/d+E_{corr} and DFTB3-OP+E_{corr} models, we computed the 2D adiabatic potential energy sugar pucker profile of the abasic ribonucleoside rH (the ribonucleoside with an abasic site, i.e., the nucleobase replaced by a hydrogen atom) using MP2/6-311++G(3df,2p)//MP2/6-31++G(d,p) and the uncorrected semi-

DOI: 10.1021/acs.jctc.7b00161
J. Chem. Theory Comput. XXXX, XXX, XXX−XXX

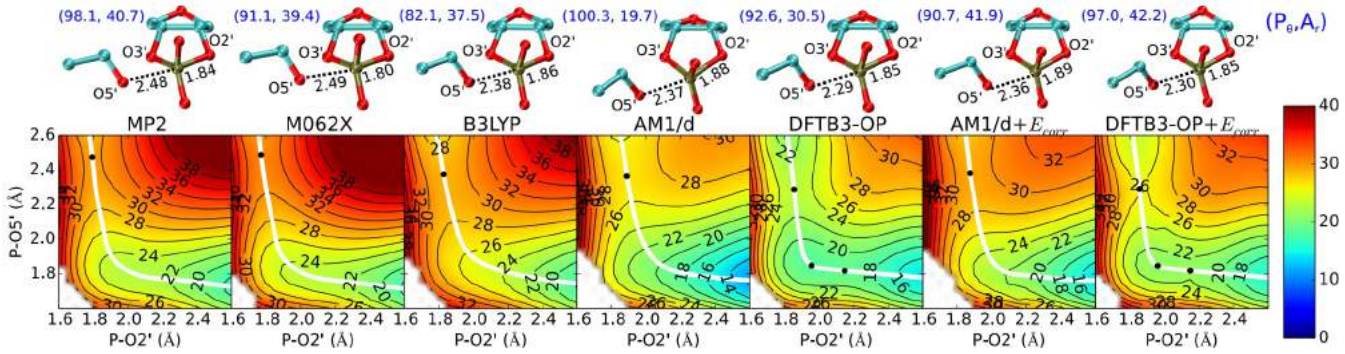

Figure 3. 2D gas-phase PESs of the EthO···SP nonenzymatic model transesterification reaction. The structures are the rate-limiting transition states. The coordinates are the nucleophile bond P−O2′ and the leaving group bond P−O5′. Stationary points along reaction paths are shown as black dots. Relative potential energies are calculated with respect to reactant energy minimum from each model (kcal/mol). Values in the parentheses are pseudorotation phase angle P_θ (deg) and puckering amplitude A_r (deg), respectively.

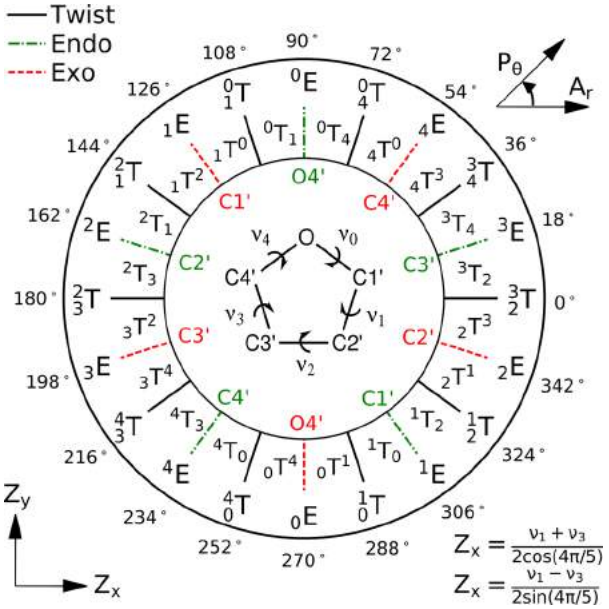

Figure 4. Pseudorotation cycle of the five-membered ring along with a furanose structure. The pseudorotation can be characterized by using the (A_r,P_θ) polar coordinates or (Z_x,Z_y) Cartesian coordinates. The relation between coordinate systems and proper torsions ν can be expressed as $Z_x = (\nu_1 + \nu_3)/(2\cos(4\pi/5))$, $Z_y = (\nu_1 - \nu_3)/(2\sin(4\pi/5))$, $P_\theta = \arctan(Z_y/Z_x)$, and $A_r = \sqrt{Z_x^2 + Z_y^2}$, where ν_1 and ν_3 are chosen to use the same starting phase angle as the convention $(P_\theta(^3_2\mathrm{T}) = 0°)$.[3] The pseudorotation names are shown along the wheel for Exo ($_nE$), Endo (^nE), and Twist (^m_nT, $_nT^m$, and ^nT_m) conformations, where m and n denotes the O4′, C1′, C2′, C3′, and C4′ atoms in respective order; the superscript/subscript position stands for the atom above/below the ideal flat five-membered ring; the atom n on the left side of T has larger displacement from the ideal flat ring than the atom m on the right side.

empirical models. The BMAP correction *is the energy difference* between the MP2 and semiempirical model rH profiles.[16]

Table 1 lists several properties for the EthO···SP reaction stationary points, including the pucker parameters P_θ and A_r (deg); sugar ring pseudorotation names (PN); forming (R2) P−O2′ and breaking (R5) P−O5′ bond lengths (Å); Gibbs free energies G (kcal/mol) and entropy contributions T·S (kcal/mol) from normal-mode analysis; the potential energy reaction barriers ΔE (kcal/mol); and the free energy barriers ΔG (kcal/mol), where MIN and TS denote the reactant state and rate-limiting transition state, respectively.

1D Free Energy Profiles of RNA Transesterification Model Reaction. The QM/MM PMF profiles of the CpA transesterification reaction in solution are shown in Figure 5. The CpA RNA (Figure 1b) was solvated in a 45.6 Å cubic box with 3021 TIP4P-Ew water molecules.[39] The net 2− charge was neutralized by adding 10 Na^+ and 8 Cl^- ions to achieve the physiological ion concentration of 0.14 M. Umbrella window sampling was performed to scan the approximate phosphoryl transfer reaction coordinate R5−R2, where R5 and R2 denote the breaking bond P−O5′ and forming bond P−O2′, respectively, using a harmonic potential force constant of 100 kcal $mol^{-1}A^{-2}$ at 96 evenly spaced distances ranging from −3.0 to 1.7 Å. Each window was equilibrated for 50 ps at constant pressure (1 bar) and temperature (300 K) before running 500 ps NVT production. Further technical details, including thermostat and particle mesh Ewald settings, are supplied in the Supporting Information.

Three sets of umbrella window simulations were performed. The "CpA_TQM, AM1/d" and "CpA_FQM, AM1/d" simulations are both evaluated with the AM1/d-PhoT semiempirical Hamiltonian, but they use different QM regions. TQM and FQM refer to the "truncated" and "full" QM regions illustrated in Figure 2. The histidines appearing in Figure 2 are RNase A residues. Those residues are not present when simulating the CpA in solution. The "CpA_FQM, AM1/d +E_{corr}" simulations include the BMAP sugar pucker correction. The MM region is evaluated with the AMBER FF10 force field[40] and TIP4P-Ew waters.[39]

Table 2 contains time-averaged values of key structural information from the simulations of the reactant (MIN) and transition state (TS) structures, including relevant bond lengths and the cytidine sugar ring pseudorotation parameters.

Figure 6 overlays the coordinates of 10 transition state structures chosen randomly from the last 50 ps of simulation.

Figure 7 compares the sampling and probability distributions of the cytidine sugar ring P_θ and A_r pseudorotation parameters between the three simulations. The corresponding figure for the adenine sugar ring is provided in the Supporting Information (Figure S1).

Simulations of CpA Catalyzed by RNase A. *Molecular Dynamics Simulations of the Reactant State.* It is of interest to ascertain whether the BMAP correction improves the AM1/d-PhoT description of sugar puckering in a large, enzymatic

DOI: 10.1021/acs.jctc.7b00161
J. Chem. Theory Comput. XXXX, XXX, XXX−XXX

Table 1. Structural and Energetic Parameters for Gas-Phase EthO···SP Nonenzymatic Model Transesterification Reaction for Different *ab Initio* and Semiempirical Quantum Models[a]

	MIN						TS							Barrier	
QM model	P_θ	A_r	PN[h]	R5	G[i]	T·S	P_θ	A_r	PN	R2	R5	G[i]	T·S	ΔE	ΔG
MP2[b]	170.4	43.3	$^2T_3$	1.72	90.00	34.78	98.1	40.7	$^0T_1$	1.84	2.48	128.28	34.79	29.88	28.28
M062X[c]	167.7	41.9	$^2T_3$	1.69	89.27	34.45	91.1	39.4	$^0T_1$	1.80	2.49	118.31	34.65	30.78	29.04
B3LYP[d]	169.3	40.2	$^2T_3$	1.72	85.75	36.11	82.1	37.5	$^0T_4$	1.86	2.38	113.56	35.61	28.87	27.81
AM1/d[e]	150.1	28.4	$^2T_1$	1.71	88.18	37.64	100.3	19.7	$^0T_1$	1.88	2.37	114.21	37.33	26.58	26.03
DFTB3- OP[f]	166.8	39.7	$^2T_3$	1.72	81.52	37.04	92.6	30.5	$^0T_1$	1.85	2.29	104.00	36.64	23.11	22.48
AM1/d+E_{corr}[g]	146.7	44.6	$^2T_1$	1.71	88.66	37.10	90.7	41.9	$^0T_1$	1.89	2.36	117.06	37.04	29.25	28.40
DFTB3-OP+E_{corr}[g]	165.8	42.3	$^2T_3$	1.72	81.84	37.13	97.0	42.2	$^0T_1$	1.85	2.30	106.29	37.21	26.02	24.45

[a]Listed are puckering parameters P_θ and A_r (deg) and pseudorotation names (PN) of the C5 sugar ring, the P−O2′ (R2), and P−O5′ (R5) bond lengths (Å), Gibbs free energies G (kcal/mol) and entropy contribution T·S (kcal/mol), adiabatic energy barriers ΔE (kcal/mol) and Gibbs free energy barriers ΔG (kcal/mol). MIN and TS denote the reactant state and rate-limiting transition state, respectively. [b]MP2/6-311++G(3df,2p)//MP2/6-31++G(d,p). [c]M062X/6-311++G(3df,2p)//M062X/6-31++G(d,p). [d]B3LYP/6-311++G(3df,2p)//B3LYP/6-31++G(d,p). [e]AM1/d-PhoT.[24] [f]DFTB3−3ob/OPhyd with the special O−P pair parameter.[33] [g]E_{corr} is an empirical correction to improve sugar pucker.[16] [h]Both $^2T_3$ and $^2T_1$ belongs to C2′-endo conformation.[3] [i]Gibbs free energies G were relative values with respect to adiabatic potential energies of the reactant.

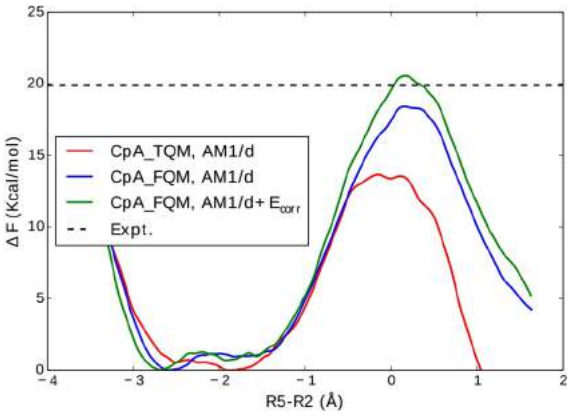

Figure 5. 1D PMF profiles of the nonenzymatic CpA model reaction. R5 and R2 denote the breaking bond P−O5′ and the forming bond P−O2′, respectively. Experimental values are indicated by dotted lines.[46]

environment. To this end, we have performed AM1/d-PhoT QM/MM simulations of the CpA reactant state when it is complexed to the RNase A protein (Figure 1c). The QM/MM simulations are performed with and without the BMAP correction, and we monitored the C5 sugar ring pseudorotation parameters. The resulting distributions of pseudorotation parameters are compared to those obtained from pure MM simulations (Figure 8). Mean values and standard deviations of the C5 sugar ring pseudorotation parameters are listed in Table 3. An analogous comparison of the A3 sugar ring pseudorotation distributions is provided in the Supporting Information (Figure S4).

The QM/MM simulations used the RNaseA_TQM QM region shown in Figure 2 and the MM region was evaluated with the AMBER FF10 force field[40] and TIP4P-Ew waters.[39]

We began by preparing the system from the experimental crystallographic structure[41] (PDBID: 1RPG) by adding 23,940 TIP4P-Ew waters and balancing the 4+ net charge with 66 Na^+ and 70 Cl^- ions to reach a 0.14 M physiological ion concentration. The system was equilibrated with the AMBER FF10 force field[40] for 12 ns at constant pressure (1 bar) and temperature (300 K) and was followed by 100 ns of MM production at constant volume and temperature (300 K); the last 75 ns of which was used for analyzing the sugar ring pseudorotation distributions.

The QM/MM simulations were performed by extracting 23 randomly selected frames from the last 1 ns of MM production. Each of the extracted frames was chosen as a starting point for a QM/MM simulation. Each of these QM/MM simulations was re-equilibrated for 50 ps at constant pressure and temperature, followed by 1.2 ns of NVT production. The 23 trajectories are concatenated and subsequently analyzed. Further technical details, including a description of the system preparation from the crystallographic structure, can be found in the Supporting Information.

2D Free Energy Profiles of Catalyzed Transphosphorylation. The QM/MM 2D PMF profiles of the CpA transesterification reaction in the RNase A enzymatic environment are shown in Figure 9. The preparation and initial MM equilibration of the RNase A system (Figure 1c) are described in the preceding section. Specifically, the final coordinates of the reactant state MM production are used to initiate the QM/MM umbrella window simulations. The two coordinates defining the PMF surface are the general acid (R_{GA} = $R_{N119-H}-R_{O5'-H}$) and phosphoryl transfer (R_{PT} = $R_{P-O5'}-R_{P-O2'}$) coordinates.[42−44] Each 2D PMF is produced from the analysis of 528 umbrella window simulations that scan the umbrella window coordinates from −2.2 to 2.2 Å in steps of 0.2 Å. The harmonic force constant was set to 100 kcal mol^{-1} $Å^{-2}$, and each window was re-equilibrated with QM/MM for 50 ps at constant pressure (1 bar) and temperature (300 K). Production statistics were then taken from 800 ps of NVT sampling. Analogous sets of 2D PMFs involving the general base (R_{GB} = $R_{O2'-H}-R_{N12-H}$) and phosphoryl transfer coordinates can be found in the Supporting Information. The Supporting Information also includes additional technical details, including the description of "histogram tests"[45] used to validate the chosen reaction coordinates.

Three sets of umbrella window simulations were performed. The "RNaseA_TQM AM1/d" and "RNaseA_FQM AM1/d" simulations are both evaluated with the AM1/d-PhoT semiempirical Hamiltonian, but they use different QM regions. TQM and FQM refer to the "truncated" and "full" QM regions illustrated in Figure 2. The histidines shown in Figure 2 are RNase A residues, and they are included in both QM regions. The "RNaseA_FQM AM1/d+E_{corr}" simulations include the BMAP sugar pucker correction.

The black dots appearing in Figure 9 are stationary points on the 2D PMF surface. The red and blue lines are minimum free

DOI: 10.1021/acs.jctc.7b00161
J. Chem. Theory Comput. XXXX, XXX, XXX−XXX

Table 2. Structural and Energetic Parameters for Solution-Phase Nonenzymatic (CpA) and Enzymatic (RNase A) Transesterification Reactions Using the AM1/d Semiempirical QM Model with Different QM/MM Truncation Schemes[a]

QM region/	QM model/	MIN		TS		MIN				TS				
Expt. System	Expt.	P_θ	A_r	P_θ	A_r	R_{N119-H}	$R_{O5'-H}$	$R_{P-O5'}$	$R_{P-O2'}$	R_{N119-H}	$R_{O5'-H}$	$R_{P-O5'}$	$R_{P-O2'}$	ΔF
CpA_TQM	AM1/d	28.8 ± 18.1	32.0 ± 6.7	127.4 ± 28.7	30.3 ± 8.1	–	–	1.66 ± 0.03	3.58 ± 0.06	–	–	1.89 ± 0.05	1.82 ± 0.04	13.6 ± 0.4
CpA_FQM	AM1/d	−11.8 ± 41.7	18.8 ± 6.9	−23.1 ± 72.0	12.3 ± 6.0	–	–	1.65 ± 0.03	4.23 ± 0.05	–	–	2.00 ± 0.06	1.79 ± 0.04	18.6 ± 0.3
CpA_FQM	AM1/d +E_{corr}	30.8 ± 15.7	44.7 ± 4.8	55.4 ± 13.1	39.8 ± 6.4	–	–	1.65 ± 0.03	4.33 ± 0.06	–	–	1.99 ± 0.06	1.80 ± 0.04	20.7 ± 0.2
UpG	Expt.[46]	–	–	–	–	–	–	–	–	–	–	–	–	19.9 ± 0.02
RNaseA_TQM[b]	AM1/d	−0.1 ± 21.4	27.0 ± 5.1	67.3 ± 9.5	36.0 ± 5.6	1.04 ± 0.03	2.03 ± 0.06	1.68 ± 0.03	3.35 ± 0.06	1.54 ± 0.05	1.13 ± 0.04	1.85 ± 0.07	3.08 ± 0.08	18.7 ± 0.3
RNaseA_FQM[b]	AM1/d	−18.3 ± 16.9	27.6 ± 5.1	−50.0 ± 40.7	17.8 ± 6.0	1.04 ± 0.03	2.10 ± 0.06	1.66 ± 0.03	3.93 ± 0.06	1.65 ± 0.05	1.09 ± 0.03	1.94 ± 0.13	3.17 ± 0.14	26.3 ± 0.4
RNaseA_FQM[b]	AM1/d +E_{corr}	18.9 ± 13.1	39.0 ± 5.4	8.5 ± 8.7	43.3 ± 3.9	1.03 ± 0.03	1.97 ± 0.06	1.68 ± 0.03	3.03 ± 0.06	1.62 ± 0.05	1.10 ± 0.03	1.87 ± 0.07	3.04 ± 0.08	23.7 ± 0.2
RNaseA_TQM[c]	AM1/d	–	–	24.7 ± 16.5	29.2 ± 5.8	–	–	–	–	1.06 ± 0.03	1.83 ± 0.05	1.93 ± 0.05	1.86 ± 0.05	22.3 ± 0.5
RNaseA_FQM[c]	AM1/d	–	–	8.8 ± 24.5	21.5 ± 6.1	–	–	–	–	1.07 ± 0.03	1.80 ± 0.05	2.15 ± 0.07	1.77 ± 0.04	20.7 ± 0.4
RNaseA_FQM[c]	AM1/d +E_{corr}	–	–	23.8 ± 12.3	35.1 ± 4.9	–	–	–	–	1.08 ± 0.03	1.73 ± 0.05	2.18 ± 0.07	1.78 ± 0.04	17.7 ± 0.4
RNase A (UpA)	Expt.[50]	–	–	–	–	–	–	–	–	–	–	–	–	13.2

[a]Listed are bond lengths R_{N119-H}, $R_{O5'-H}$, $R_{P-O5'}$, and $R_{P-O2'}$ (Å), cytidine sugar ring P_θ and A_r (deg) pseudorotation parameters, and the reaction free energy barriers ΔF (kcal/mol). MIN and TS stand for the reactant minimum and transition state, respectively. RNaseA_TQM and RNaseA_FQM denote the truncated and full QM regions used in QM/MM simulations (Figure 2). [b]Mechanism along lower-right (LowR) path with an early TS. [c]Mechanism along upper-left (UpL) path with a late TS. Note: Data for the MIN state is identical to that for the LowR path listed above and therefore is not shown.

J. Chem. Theory Comput. XXXX, XXX, XXX−XXX DOI: 10.1021/acs.jctc.7b00161

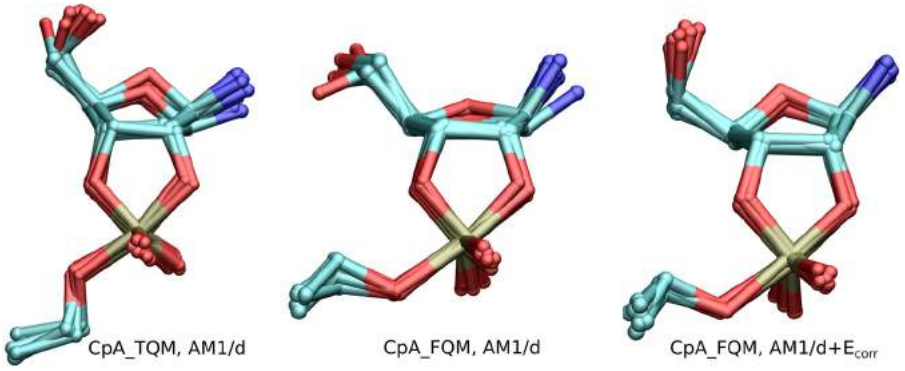

Figure 6. Coordinate overlay of approximate transition state structures from the nonenzymatic CpA model reaction simulations. The hydrogen atoms and cytosine and adenosine groups are removed to improve clarity.

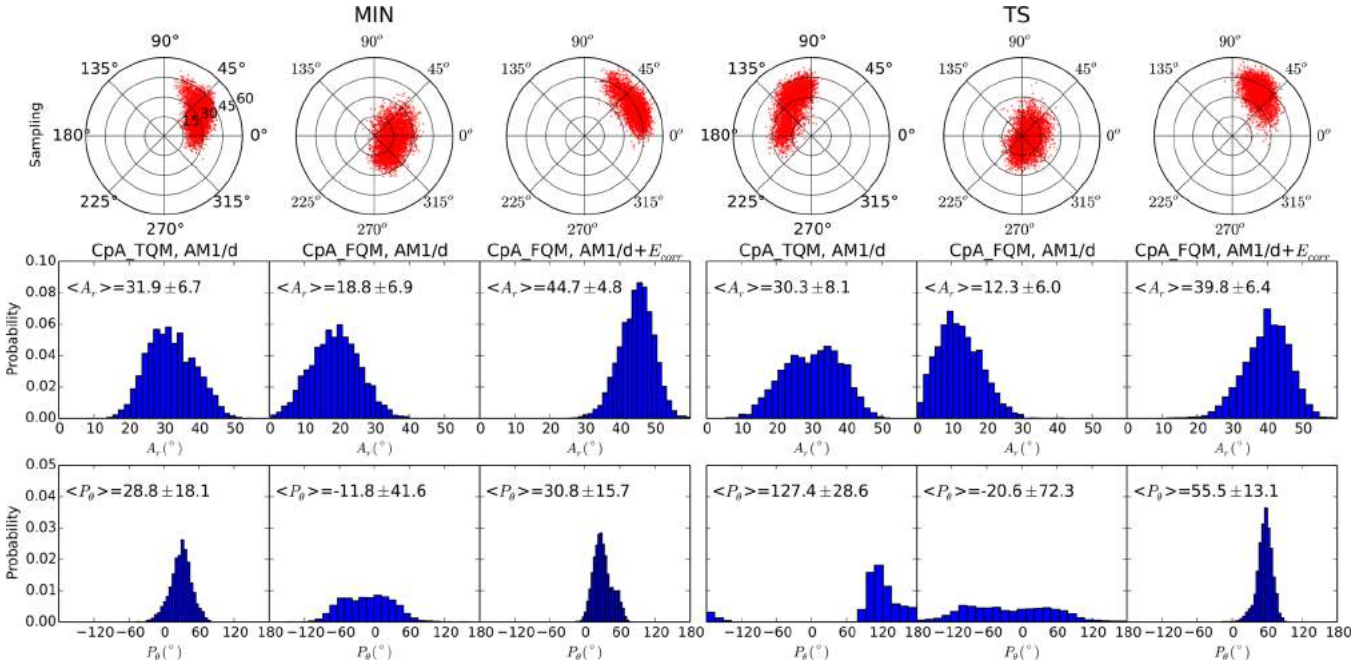

Figure 7. Sampling, probability distributions, and statistical values of the P_θ and A_r (deg) pseudorotation parameters for the CpA cytidine sugar ring. MIN and TS denote reactant and transition states, respectively.

energy pathways connecting the reactant and product states, as determined from NEB optimization on the 2D PMF surface. The red and blue lines in the 1D plots within Figure 9 are merely the projections of the 2D PMF along the corresponding NEB paths. "LowR" and "UpL" are abbreviations for the "lower right" and "upper left" NEB paths, respectively.

Table 2 contains time-averaged values of key structural information from the simulations of the reactant (MIN) and the two transition state (TS) structures, including relevant bond lengths and the cytidine sugar ring pseudorotation parameters.

RESULTS AND DISCUSSION

RNA Transesterification Minimal Model (EthO···SP) in the Gas Phase. The 2D gas-phase adiabatic potential energy surfaces and late transition state structures for the minimal EthO···SP nonenzymatic RNA transesterification reaction model are shown in Figure 3 for several *ab initio* and semiempirical quantum models. Close barriers are observed in the *ab initio* potential energy profiles. The late transition state is characterized by a longer breaking bond R5 and a shorter forming bond R2 as listed in Table 1, characteristic of an associative asynchronous mechanism for the model reaction.[17,26,27] The AM1/d profile is in close agreement with the MP2 and DFT results. The DFTB3-OP energy profiles are similar to the MP2 and DFT results but predict an associative stepwise mechanism with a metastable intermediate.[17] Figure 3 and Table 1 show that the semiempirical methods systematically predict similar sugar ring pseudorotation phase angles but smaller ring puckering amplitudes and reaction barriers than MP2. The AM1/d and DFTB3-OP adiabatic potential (free energy) barriers are less than MP2 by 3.30 (2.25) and 6.77 (5.80) kcal/mol, respectively. The corrected semiempirical models greatly improve sugar ring puckering amplitudes, which are in excellent agreement with MP2 results. The enhanced puckering amplitudes lead to better sugar ring conformations of stationary points and improved reaction barriers; the corrected AM1/d and DFTB3-OP adiabatic potential (free energy) barriers are less than MP2 by 0.63 (−0.12) and 3.86 (3.84) kcal/mol, respectively, which are in considerably better agreement with the MP2 results than the uncorrected potentials.

DOI: 10.1021/acs.jctc.7b00161
J. Chem. Theory Comput. XXXX, XXX, XXX−XXX

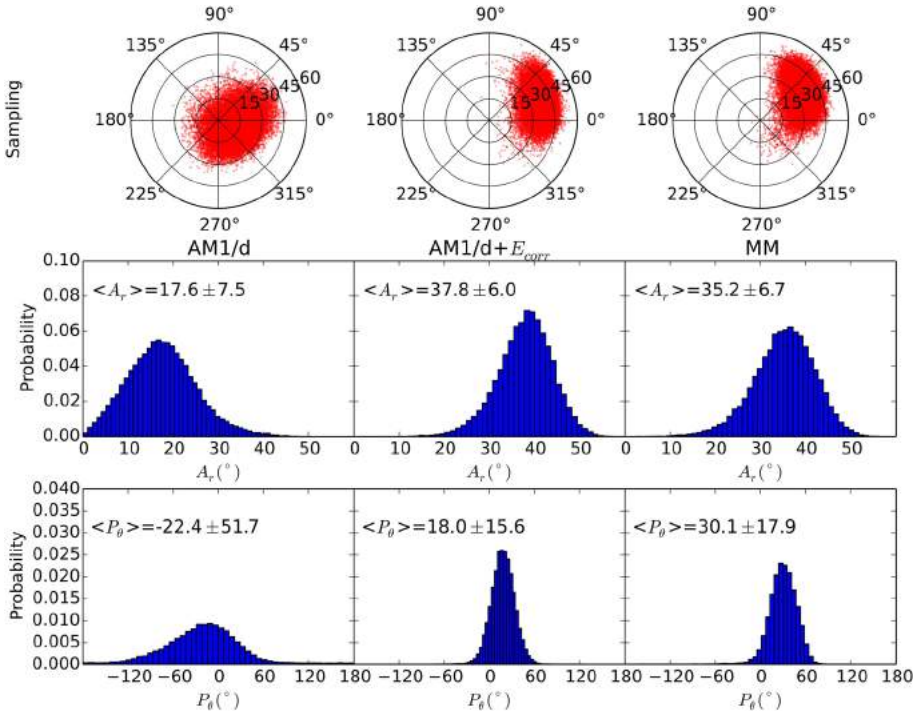

Figure 8. Sampling, probability distributions, and statistical analysis of the P_θ and A_r (deg) pseudorotation parameters from the RNase A reactant state C5 sugar ring.

Table 3. Statistics for Sugar Pucker Parameters from Simulations of the RNase A Reactant State[a]

Model	P_θ	A_r
AM1/d	−22.4 ± 51.7	17.6 ± 7.5
AM1/d + E_{corr}	18.0 ± 15.6	37.8 ± 6.0
AMBER MM	30.1 ± 17.9	35.2 ± 6.7

[a]Listed are mean values and their standard deviations for pseudorotation parameters P_θ and A_r (deg) of residue C5 sugar ring for QM/MM simulations using the AM1/d and corrected AM1/d +E_{corr} QM models and conventional MM simulations with AMBER (see Computational Methods section for details).

Nonenzymatic CpA Transesterification. The 1D free energy profiles of the nonenzymatic CpA transesterification reaction model (Figure 5) show that simulations with truncated CpA as the QM region (CpA_TQM) predict a lower free energy barrier than simulations with full CpA (CpA_FQM) as the QM region by 5−7 kcal/mol, suggesting that the entire CpA may be required to be treated with QM to obtain accurate reaction free energy barriers.

Table 2 shows that reaction free energy barriers predicted with AM1/d and AM1/d+E_{corr} models for CpA_FQM system are 18.6 ± 0.4 and 20.7 ± 0.2 kcal/mol, respectively. The result indicates that the introduction of sugar pucker correction into the semiempirical AM1/d model increases reaction free energy barrier of CpA transesterification by 2.1 kcal/mol, which is in better agreement with the experimental value of 19.9 ± 0.02 kcal/mol.[46] CpA transesterification occurs via a concerted mechanism with a slightly late TS as shown in Figure 5.[26,27]

Figure 7 and Table 2 show that the corrected semiempirical AM1/d method greatly enhances sugar ring conformations of the reactant (MIN) and transition state (TS). The regular AM1/d method predicts small puckering amplitudes (less than 20°) and large standard deviations (more than 40°) for pseudorotation phase angles of cytidine sugar rings due to almost flat sugar rings (Figure 6). The sugar rings modeled by AM1/d for CpA_TQM and AM1/d+E_{corr} for CpA_FQM have qualitatively correct puckered conformations as shown in Figures 7 and 6, the former correctly predicting slightly smaller puckering amplitudes and larger standard deviations of the pseudorotation phase angle.

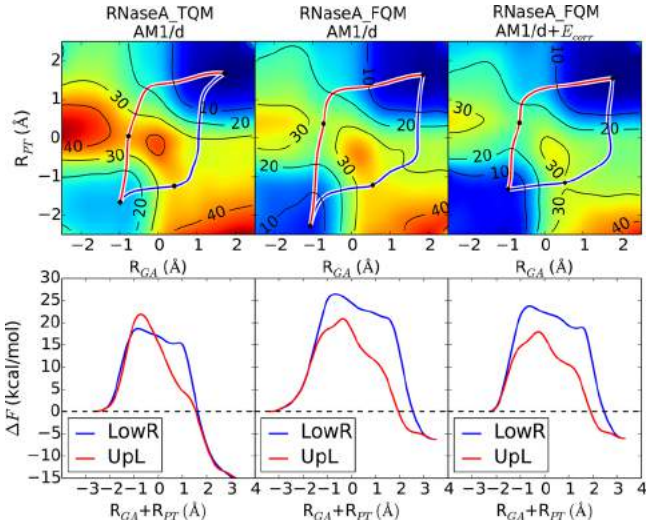

Figure 9. 2D PMFs of the enzymatic RNase A transphosphorylation reaction and their 1D projections. Stationary points along reaction paths are shown as black dots. R_{GA} and R_{PT} denote the reaction coordinates for general acid step (R_{N119-H}−$R_{O5'-H}$) and phosphate transfer step ($R_{P-O5'}$−$R_{P-O2'}$), respectively. LowR and UpL paths stand for the lower-right and upper-left asynchronous concerted mechanisms, respectively. RNaseA_TQM and RNaseA_FQM denote truncated and full CpA as QM regions in QM/MM simulations (Figure 2).

DOI: 10.1021/acs.jctc.7b00161
J. Chem. Theory Comput. XXXX, XXX, XXX−XXX

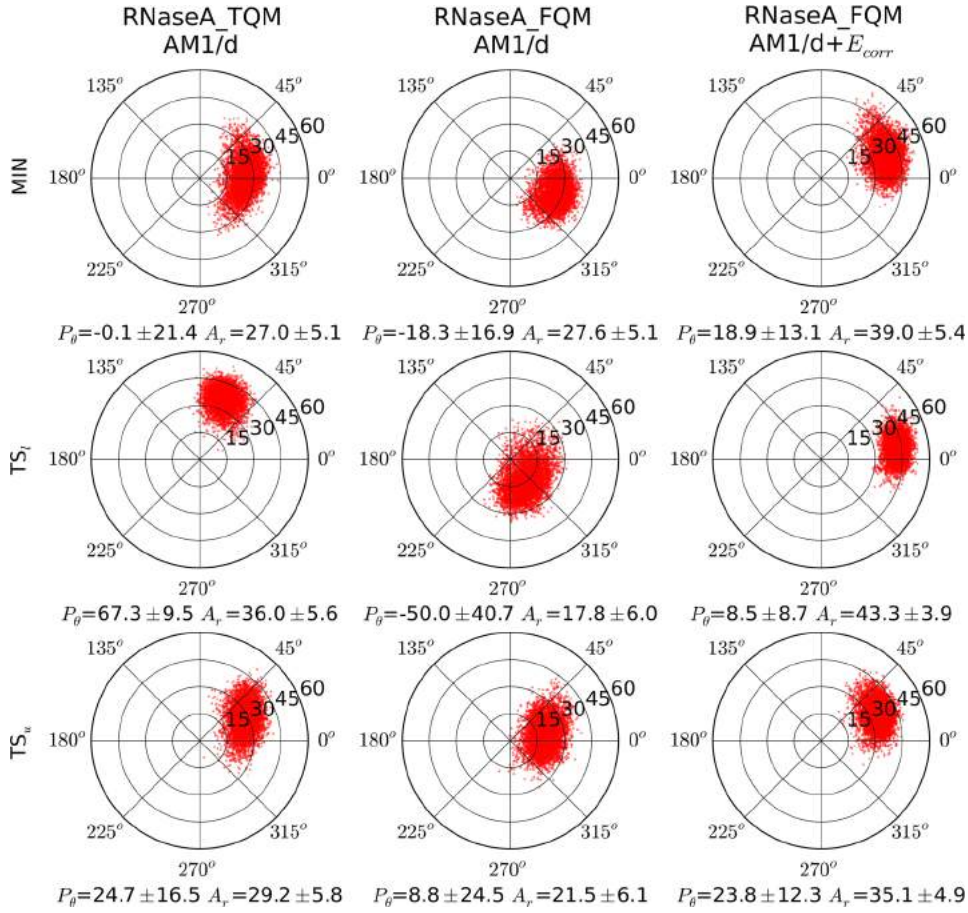

Figure 10. Sampling, mean values and standard deviations of the P_θ and A_r (deg) pseudorotation parameters from the C5 sugar ring in the RNase A reactant state (MIN) and transition states (TS_l and TS_u). TS_l and TS_u denote transition states along lower-right and upper-left asynchronous concerted paths, respectively (Figure 9). RNaseA_TQM and RNaseA_FQM mean truncated and full CpA as QM regions in QM/MM simulations (Figure 2).

Enzymatic RNase A Transesterification. *Conformational Dynamics of RNase A Reactant State.* Figure 8 illustrates the sugar puckering parameter distributions for the C5 residue in the RNase A reactant state MD simulations using MM, AM1/d, and corrected AM1/d models. The distributions of phase angle and puckering amplitude for the AM1/d differ significantly from the MM. The standard deviation (51.7°) of AM1/d pseudorotation phase angle is more than three times larger than the MM result (15.6°), and the average AM1/d puckering amplitude (17.6 ± 7.5°) is almost half of the MM reference (35.2 ± 6.7°), indicating that AM1/d predicts a nearly flat sugar ring. The corrected AM1/d method, on the other hand, reasonably reproduces the MM sugar puckering phase and amplitude distributions.

Catalyzed Transphosphorylation. Figure 9 shows that each 2D free energy landscape of RNase A transphosphorylation has two minima, the lower-left reactant (MIN) and the upper-right product, which are connected by two possible reaction paths, the upper-left path (UpL) and the lower-right one (LowR), respectively. The UpL profile describes a path where phosphoryl transfer first advances and proton transfer from the general acid is late. Alternatively, the LowR profile describes a path where proton transfer occurs first, followed by phosphoryl transfer.

1D projections of two reaction paths in the 2D free energy landscapes in Figure 9 show that different QM truncation schemes lead to different favored reaction paths/mechanisms. Simulations with RNaseA_TQM truncation predict that the UpL and LowR paths have similar barriers, with LowR slightly lower, whereas the RNaseA_FQM simulations, with and without sugar pucker correction, indicate the UpL pathways to be considerably more favorable. Previous experimental and theoretical studies support the UpL mechanism,[30,47,48] suggesting that the results with full QM treatment of the dinucleotide CpA are important.

Although the simulations with RNaseA_FQM described by AM1/d model can correctly predict the reaction path, sugar ring conformations are poor, as shown in Figure 10, and are significantly improved with the AM1/d+E_{corr} model.

Figure 9 shows that simulations with RNaseA_FQM as the QM region described by both AM1/d and AM1/d+E_{corr} predict the experimentally supported mechanism, but AM1/d+E_{corr} predicts a lower free energy barrier (17.7 kcal/mol) than AM1/d by 3 kcal/mol and is in better agreement with the value estimated from experiment of 13.2 kcal/mol.[49,50] The decrease in the free energy barrier with AM1/d+E_{corr} can be attributed to the structural change of the reactant, which gets closer in structure to the TS as shown in Figure 2 and Table 2 due to the improved sugar puckering. The AM1/d+E_{corr} method predicts larger puckering amplitude of the C5 sugar ring and a shorter P−O2′ bond.

DOI: 10.1021/acs.jctc.7b00161
J. Chem. Theory Comput. XXXX, XXX, XXX−XXX

CONCLUSIONS

Recent studies have shown that conventional uncorrected semiempirical quantum mechanical methods fail to adequately describe the DNA and RNA sugar puckers, which play a significant role in nucleic acid structure and function and can influence their interactions with proteins. In this work, a BMAP correction term is used that leads to significant improvement in the proper modeling of sugar ring. This correction was further applied to study RNA transesterification reaction models including RNase A catalysis and was demonstrated to provide considerably improved behavior and predictions. The BMAP corrections are shown to improve prediction of the QM/MM free energy barriers of both nonenzymatic and enzymatic transesterification reactions. The simulations of CpA transesterification in both nonenzymatic and enzymatic environments underscore the sensitivity of results to the size of the QM region and in some cases may require consideration of the entire (CpA) dinucleotide for the best results with these QM models. These results demonstrate that the sugar pucker correction is useful for QM/MM simulations of RNA with semiempirical quantum mechanical methods.

ASSOCIATED CONTENT

Supporting Information

The Supporting Information is available free of charge on the ACS Publications website at DOI: 10.1021/acs.jctc.7b00161.

General settings for molecular dynamics simulations, simulation details, convergence tests, and sampling overlaps of RNA transesterification model reactions and RNase A system, simulation results on adenine residue and RNase A transphosphorylation along the general base and phosphate transfer steps, and histogram test for reaction coordinates/paths of RNase A transesterifications. (PDF)

AUTHOR INFORMATION

Corresponding Author

*E-mail: Darrin.York@rutgers.edu.

ORCID

Ming Huang: 0000-0001-7367-3626
Brian K. Radak: 0000-0001-8628-5972
Tai-Sung Lee: 0000-0003-2110-2279
Darrin M. York: 0000-0002-9193-7055

Notes

The authors declare no competing financial interest.

ACKNOWLEDGMENTS

The authors are grateful for financial support provided by the National Institutes of Health (No. GM107485). Computational resources were provided by the National Institutes of Health under Grant No. S10OD012346 and by the Extreme Science and Engineering Discovery Environment (XSEDE), which is supported by National Science Foundation Grant No. OCI-1053575 (Project No. TG-MCB110101). This work benefited from access to RDI2 Research Instruments.

REFERENCES

(1) Varki, A., Cummings, R. D., Esko, J. D., Freeze, H. H., Stanley, P., Bertozzi, C. R., Hart, G. W., Etzler, M. E., Eds.; *Essentials of Glycobiology*, 2nd ed.; Cold Spring Harbor: New York, 2009; Chapter 1, pp 1−22.

(2) Bloomfield, V. A.; Crothers, D. M.; Tinoco, I., Jr. *Nucleic Acids: Structures, Properties, and Functions*; University Science Books: Sausalito, CA, 2000; Chapters 2 and 5, pp 13−44, 111−164.

(3) Saenger, W. *Principles of Nucleic Acid Structure*; Springer-Verlag: New York, 1984; Chapters 2 and 17, pp 17−21, 368−384.

(4) Rich, A. The double helix: a tale of two puckers. *Nat. Struct. Biol.* **2003**, *10*, 247−249.

(5) Murray, L. J. W.; Arendall, W. B.; Richardson, D. C.; Richardson, J. S. RNA backbone is rotameric. *Proc. Natl. Acad. Sci. U. S. A.* **2003**, *100*, 13904−13909.

(6) Tolstorukov, M. Y.; Jernigan, R. L.; Zhurkin, V. B. Protein-DNA Hydrophobic Recognition in the Minor Groove is Facilitated by Sugar Switching. *J. Mol. Biol.* **2004**, *337*, 65−76.

(7) Julien, K. R.; Sumita, M.; Chen, P.-H.; Laird-Offringa, I. A.; Hoogstraten, C. G. Conformationally restricted nucleotides as a probe of structure-function relationships in RNA. *RNA* **2008**, *14*, 1632−1643.

(8) Zhang, N.; Zhang, S.; Szostak, J. W. Activated ribonucleotides undergo a sugar pucker switch upon binding to a single-stranded RNA template. *J. Am. Chem. Soc.* **2012**, *134*, 3691−3694.

(9) Taha, H. A.; Richards, M. R.; Lowary, T. L. Conformational Analysis of Furanoside-Containing Mono- and Oligosaccharides. *Chem. Rev.* **2013**, *113*, 1851−1876.

(10) Li, L.; Szostak, J. W. The Free Energy Landscape of Pseudorotation in 3′-5′ and 2′-5′ Linked Nucleic Acids. *J. Am. Chem. Soc.* **2014**, *136*, 2858−2865.

(11) Mayes, H. B.; Broadbelt, L. J.; Beckham, G. T. How Sugars Pucker: Electronic Structure Calculations Map the Kinetic Landscape of Five Biologically Paramount Monosaccharides and Their Implications for Enzymatic Catalysis. *J. Am. Chem. Soc.* **2014**, *136*, 1008−1022. PMID: 24368073.

(12) Casanovas, J.; Revilla-López, G.; Bertran, O.; del Valle, L. J.; Turon, P.; Puiggalí, J.; Alemán, C. Restricted Puckering of Mineralized RNA-Like Riboses. *J. Phys. Chem. B* **2014**, *118*, 5075−5081. PMID: 24787993.

(13) Radak, B. K.; Romanus, M.; Lee, T.-S.; Chen, H.; Huang, M.; Treikalis, A.; Balasubramanian, V.; Jha, S.; York, D. M. Characterization of the Three-Dimensional Free Energy Manifold for the Uracil Ribonucleoside from Asynchronous Replica Exchange Simulations. *J. Chem. Theory Comput.* **2015**, *11*, 373−377.

(14) Pshetitsky, Y.; Eitan, R.; Verner, G.; Kohen, A.; Major, D. T. Improved Sugar Puckering Profiles for Nicotinamide Ribonucleoside for Hybrid QM/MM Simulations. *J. Chem. Theory Comput.* **2016**, *12*, 5179−5189.

(15) Barnett, C. B.; Naidoo, K. J. Ring Puckering: A Metric for Evaluating the Accuracy of AM1, PM3, PM3CARB-1, and SCC-DFTB Carbohydrate QM/MM Simulations. *J. Phys. Chem. B* **2010**, *114*, 17142−17154.

(16) Huang, M.; Giese, T. J.; Lee, T.-S.; York, D. M. Improvement of DNA and RNA Sugar Pucker Profiles from Semiempirical Quantum Methods. *J. Chem. Theory Comput.* **2014**, *10*, 1538−1545.

(17) Huang, M.; Giese, T. J.; York, D. M. Nucleic acid reactivity: Challenges for next-generation semiempirical quantum models. *J. Comput. Chem.* **2015**, *36*, 1370−89.

(18) MacKerell, A. D., Jr.; Bashford, D.; Bellott, M.; Dunbrack, R. L., Jr.; Evanseck, J. D.; Field, M. J.; Fischer, S.; Gao, J.; Guo, H.; Ha, S.; Joseph-McCarthy, D.; Kuchnir, L.; Kuczera, K.; Lau, F. T. K.; Mattos, C.; Michnick, S.; Ngo, T.; Nguyen, D. T.; Prodhom, B.; Reiher, W. E., III; Roux, B.; Schlenkrich, M.; Smith, J. C.; Stote, R.; Straub, J.; Watanabe, M.; Wiórkiewicz-Kuczera, J.; Yin, D.; Karplus, M. All-atom empirical potential for molecular modeling and dynamics studies of proteins. *J. Phys. Chem. B* **1998**, *102*, 3586−3616.

(19) Feig, M.; MacKerell, A. D., Jr.; Brooks, C. L., III Force field influence on the observation of π-helical protein structures in molecular dynamics simulations. *J. Phys. Chem. B* **2003**, *107*, 2831−2836.

(20) MacKerell, A. D., Jr.; Feig, M.; Brooks, C. L. Improved Treatment of the Protein Backbone in Empirical Force Fields. *J. Am. Chem. Soc.* **2004**, *126*, 698−699.

DOI: 10.1021/acs.jctc.7b00161
J. Chem. Theory Comput. XXXX, XXX, XXX−XXX

(21) Buck, M.; Bouguet-Bonnet, S.; Pastor, R. W.; MacKerell, A. D., Jr. Importance of the CMAP correction to the CHARMM22 protein force field: dynamics of hen lysozyme. *Biophys. J.* **2006**, *90*, L36−L38.
(22) Hu, Y.; Ou, S.; Patel, S. Free Energetics of Arginine Permeation into Model DMPC Lipid Bilayers: Coupling of Effective Counterion Concentration and Lateral Bilayer Dimensions. *J. Phys. Chem. B* **2013**, *117*, 11641−11653.
(23) Dral, P. O.; Wu, X.; Spörkel, L.; Koslowski, A.; Thiel, W. Semiempirical Quantum-Chemical Orthogonalization-Corrected Methods: Benchmarks for Ground-State Properties. *J. Chem. Theory Comput.* **2016**, *12*, 1097−1120. PMID: 26771261.
(24) Nam, K.; Cui, Q.; Gao, J.; York, D. M. Specific reaction parametrization of the AM1/d Hamiltonian for phosphoryl transfer reactions: H, O, and P atoms. *J. Chem. Theory Comput.* **2007**, *3*, 486−504.
(25) Radak, B. K.; Harris, M. E.; York, D. M. Molecular simulations of RNA 2′-*O*-transesterification reaction models in solution. *J. Phys. Chem. B* **2013**, *117*, 94−103.
(26) Huang, M.; York, D. M. Linear free energy relationships in RNA transesterification: theoretical models to aid experimental interpretations. *Phys. Chem. Chem. Phys.* **2014**, *16*, 15846−15855.
(27) Chen, H.; Giese, T. J.; Huang, M.; Wong, K.-Y.; Harris, M. E.; York, D. M. Mechanistic Insights into RNA Transphosphorylation from Kinetic Isotope Effects and Linear Free Energy Relationships of Model Reactions. *Chem. Eur. J.* **2014**, *20*, 14336−14343.
(28) Chen, H.; Piccirilli, J. A.; Harris, M. E.; York, D. M. Effect of Zn^{2+} binding and enzyme active site on the transition state for RNA 2′-O-transphosphorylation interpreted through kinetic isotope effects. *Biochim. Biophys. Acta, Proteins Proteomics* **2015**, *1854*, 1795−1800.
(29) Formoso, E.; Matxain, J. M.; Lopez, X.; York, D. M. Molecular dynamics simulation of bovine pancreatic ribonuclease A-CpA and transition state-like complexes. *J. Phys. Chem. B* **2010**, *114*, 7371−7382.
(30) Gu, H.; Zhang, S.; Wong, K.-Y.; Radak, B. K.; Dissanayake, T.; Kellerman, D. L.; Dai, Q.; Miyagi, M.; Anderson, V. E.; York, D. M.; Piccirilli, J. A.; Harris, M. E. Experimental and computational analysis of the transition state for ribonuclease A-catalyzed RNA 2′-*O*-transphosphorylation. *Proc. Natl. Acad. Sci. U. S. A.* **2013**, *110*, 13002−13007.
(31) Panteva, M. T.; Dissanayake, T.; Chen, H.; Radak, B. K.; Kuechler, E. R.; Giambaşu, G. M.; Lee, T.-S.; York, D. M. In *Multiscale Methods for Computational RNA Enzymology*; Chen, S.-J., Burke-Aguero, D. H., Eds.; Elsevier, 2015; Chapter 14.
(32) Chen, H. Multiscale Simulation of RNA Catalysis. Ph.D. Thesis, Rutgers University, 2017.
(33) Gaus, M.; Lu, X.; Elstner, M.; Cui, Q. Parameterization of DFTB3/3OB for Sulfur and Phosphorus for Chemical and Biological Applications. *J. Chem. Theory Comput.* **2014**, *10*, 1518−1537.
(34) Case, D.; Babin, V.; Berryman, J.; Betz, R.; Cai, Q.; Cerutti, D.; Cheatham, T., III; Darden, T.; Duke, R.; Gohlke, H.; Goetz, A.; Gusarov, S.; Homeyer, N.; Janowski, P.; Kaus, J.; Kolossváry, I.; Kovalenko, A.; Lee, T.; LeGrand, S.; Luchko, T.; Luo, R.; Madej, B.; Merz, K.; Paesani, F.; Roe, D.; Roitberg, A.; Sagui, C.; Salomon-Ferrer, R.; Seabra, G.; Simmerling, C.; Smith, W.; Swails, J.; Walker, R.; Wang, J.; Wolf, R.; Wu, X.; Kollman, P. *AMBER 14* ; University of California, San Francisco: San Francisco, CA, 2014.
(35) Frisch, M. J.; Trucks, G. W.; Schlegel, H. B.; Scuseria, G. E.; Robb, M. A.; Cheeseman, J. R.; Scalmani, G.; Barone, V.; Mennucci, B.; Petersson, G. A.; Nakatsuji, H.; Caricato, M.; Li, X.; Hratchian, H. P.; Izmaylov, A. F.; Bloino, J.; Zheng, G.; Sonnenberg, J. L.; Hada, M.; Ehara, M.; Toyota, K.; Fukuda, R.; Hasegawa, J.; Ishida, M.; Nakajima, T.; Honda, Y.; Kitao, O.; Nakai, H.; T, V.; Montgomery, J. A., Jr.; Peralta, J. E.; Ogliaro, F.; Bearpark, M.; Heyd, J. J.; Brothers, E.; Kudin, K. N.; Staroverov, V. N.; Kobayashi, R.; Normand, J.; Raghavachari, K.; Rendell, A.; Burant, J. C.; Iyengar, S. S.; Tomasi, J.; Cossi, M.; Rega, N.; Millam, J. M.; Klene, M.; Knox, J. E.; Cross, J. B.; Bakken, V.; Adamo, C.; Jaramillo, J.; Gomperts, R.; Stratmann, R. E.; Yazyev, O.; Austin, A. J.; Cammi, R.; Pomelli, C.; Ochterski, J. W.; Martin, R. L.; Morokuma, K.; Zakrzewski, V. G.; Voth, G. A.; Salvador, P.; Dannenberg, J. J.; Dapprich, S.; Daniels, A. D.; Farkas, O.; Foresman, J. B.; Ortiz, J. V.; Cioslowski, J.; Fox, D. J. *Gaussian 09*, Revision A.02. Gaussian, Inc., Wallingford, CT, 2009.
(36) Lee, T.-S.; Radak, B. K.; Pabis, A.; York, D. M. A new maximum likelihood approach for free energy profile construction from molecular simulations. *J. Chem. Theory Comput.* **2013**, *9*, 153−164.
(37) Lee, T.-S.; Radak, B. K.; Huang, M.; Wong, K.-Y.; York, D. M. Roadmaps through free energy landscapes calculated using the multidimensional vFEP approach. *J. Chem. Theory Comput.* **2014**, *10*, 24−34.
(38) Henkelman, G.; Jónsson, H. A dimer method for finding saddle points on high dimensional potential surfaces using only first derivatives. *J. Chem. Phys.* **1999**, *111*, 7010−7022.
(39) Horn, H. W.; Swope, W. C.; Pitera, J. W.; Madura, J. D.; Dick, T. J.; Hura, G. L.; Head-Gordon, T. Development of an improved four-site water model for biomolecular simulations: TIP4P-Ew. *J. Chem. Phys.* **2004**, *120*, 9665−9678.
(40) Hornak, V.; Abel, R.; Okur, A.; Strockbine, B.; Roitberg, A.; Simmerling, C. Comparison of Multiple Amber Force Fields and Development of Improved Protein Backbone Parameters. *Proteins: Struct., Funct., Genet.* **2006**, *65*, 712−725.
(41) Zegers, I.; Maes, D.; Dao-Thi, M.-H.; Poortmans, F.; Palmer, R.; Wyns, L. The structures of RNase A complexed with 3′-CMP and d(CpA): Active site conformation and conserved water molecules. *Protein Sci.* **1994**, *3*, 2322−2339.
(42) Ganguly, A.; Thaplyal, P.; Rosta, E.; Bevilacqua, P. C.; Hammes-Schiffer, S. Quantum Mechanical/Molecular Mechanical Free Energy Simulations of the Self-Cleavage Reaction in the Hepatitis Delta Virus Ribozyme. *J. Am. Chem. Soc.* **2014**, *136*, 1483−1496.
(43) Zhang, S.; Ganguly, A.; Goyal, P.; Bingaman, J. L.; Bevilacqua, P. C.; Hammes-Schiffer, S. Role of the active site guanine in the *glmS* ribozyme self-cleavage mechanism: Quantum mechanical/molecular mechanical free energy simulations. *J. Am. Chem. Soc.* **2015**, *137*, 784−798.
(44) Radak, B. K.; Lee, T.-S.; Harris, M. E.; York, D. M. Assessment of metal-assisted nucleophile activation in the hepatitis delta virus ribozyme from molecular simulation and 3D-RISM. *RNA* **2015**, *21*, 1566−1577.
(45) Peters, B. Using the histogram test to quantify reaction coordinate error. *J. Chem. Phys.* **2006**, *125*, 241101−241104.
(46) Harris, M. E.; Dai, Q.; Gu, H.; Kellerman, D. L.; Piccirilli, J. A.; Anderson, V. E. Kinetic isotope effects for RNA cleavage by 2 ′-O-transphosphorylation: Nucleophilic activation by specific base. *J. Am. Chem. Soc.* **2010**, *132*, 11613−11621.
(47) Raines, R. T. Ribonuclease A. *Chem. Rev.* **1998**, *98*, 1045−1066.
(48) Elsässer, B.; Fels, G.; Weare, J. H. QM/MM Simulation (B3LYP) of the RNase A Cleavage-Transesterification Reaction Supports a Triester AN+DN Associative Mechanism with an O2′ H Internal Proton Transfer. *J. Am. Chem. Soc.* **2014**, *136*, 927−936.
(49) delCardayré, S. B.; Raines, R. T. Structural Determinants of Enzymic Processivity. *Biochemistry* **1994**, *33*, 6031−6037.
(50) Thompson, J. E.; Kutateladze, T.; Schuster, M.; Venegas, F.; Messmore, J.; Raines, R. Limits to Catalysis by Ribonuclease A. *Bioorg. Chem.* **1995**, *23*, 471−481.

DOI: 10.1021/acs.jctc.7b00161
J. Chem. Theory Comput. XXXX, XXX, XXX−XXX